Executive Summary of the Thesis

Aerodynamic analysis of cyclists: a novel approach combining CFD and rigging animation technique

Laurea Magistrale in Aeronautical Engineering - Ingegneria Aeronautica

Author: Giacomo Antenucci

Advisor: Prof. Paolo Schito

Co-advisors: Marco Rossoni Claudio Somaschini

Academic year: 2022-2023

1. Introduction

One of the crucial aspects of improving cycling racing performance lies in the study of aerodynamics, as nearly the 90% of the total resistance force encountered by an athlete is attributed to aerodynamic drag [3]. Currently, cyclists rely on wind tunnel tests, Computational Fluid Dynamics, or velodrome tests for investigating aerodynamics. However, wind tunnel tests remain the gold standard for aerodynamic analysis, as they allow for precise measurement of drag, side force, and other flow-related parameters, with controlled direction and intensity of the airflow. Although this procedure is reliable, it is time-consuming and resource-intensive. Cyclists are limited by the availability of wind tunnels and their busy schedules, as wind tunnel tests usually take one or two full days. Consequently, changes in position or equipment cannot be made immediately and may take weeks or even months. Additionally, wind tunnel testing requires a significant financial investment, so careful consideration must be given to test selection. Some of these issues have been addressed by leveraging 3D scan technology. Professional cyclists and teams have used it to obtain a virtual copy of the athlete [5], which is then 3D printed to create a mannequin that can be used for wind tunnel analysis without the need for the real athlete to be present. This paper aims to develop a workflow that reduces the time spent on tests by integrating CFD analysis and wind tunnel validation with 3D scanning of the cyclist and rigging animation techniques, which belong to digital animation. This allows for the virtual creation of a skeleton for the model in Blender software, which can be moved into any desired position. The research is structured as follows: Section 2 describes the procedure from the scan of a standing mannequin to the 3D printing of the cyclist position, obtained through rigging, and suitable for wind tunnel tests, illustrated in Section 3. Section 4 presents the CFD model used for grid independence, wind tunnel comparison, and analysis of six different cyclist positions. Finally, Section 5 provides the conclusions.

2. Methodology

3D scanning

The work began with the scanning of a full-size mannequin available at Politecnico di Milano. The mannequin had a height of approximately

1.80 m and was scanned in a standing position using the Artec Leo 3D scanner. The scanning process involved five scans: one for the entire body and four additional scans to capture the two removable arms, the foot, and the head. The point clouds generated from the scans were post-processed in scanning software. The necessary steps included aligning the frames and deleting those that did not meet the required accuracy of 1 mm, significantly reducing the data weight. The 3D polygonal model was then created using the smooth fusion algorithm, which combines and solidifies the captured frames. After filling any holes in the mesh, the model was ready for further analysis.

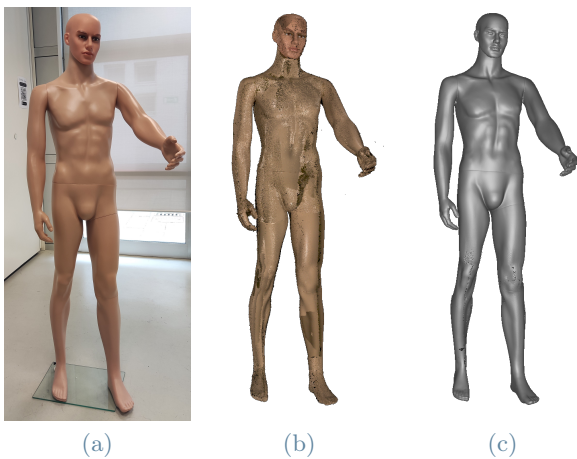(a)   (b)   (c)

Figure 1: Evolution of mannequin representation: (a) physical mannequin used as a reference, (b) scanned frames and (c) final 3D model generated by the smooth fusion.

Rigging

The rigging technique was implemented in Blender to transition the mannequin from its original standing position to a cyclist position on the bike. In the realm of digital animation, rigging involves representing the character in two components: the surface representation of the model (the mesh) and a hierarchical arrangement of interconnected digital bones (the rig or skeleton) used for creating motion [1]. The default rig provided in Blender greatly facilitated the process, consisting of 25 bones distributed throughout the body and an additional 40 bones for the hands.
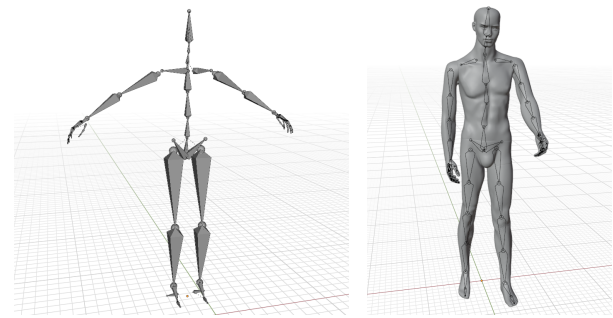

Figure 2: Default rig isolated, representing the standard skeletal structure and fitted rig applied to the mannequin.

Although this approximation falls short of the actual 206 bones present in the human body, the movements were accurately recreated by manipulating, rotating, and scaling the bones of the skeleton. Each bone was then placed in its corresponding location along the mannequin. Once the various hinges of the bones were correctly aligned to mimic the real human joints, the rig was generated. An important aspect of the process involved the weight system, which influenced how the mesh areas of the body deformed in response to the motion of each bone. The weight painting system automatically generated the necessary corrections, assigning values ranging from 1.0 (indicating full deformation following bone movement) to 0.0 (no deformation). With this step completed, the mannequin was ready to be animated using forward kinematics (imposing desired rotations on the bones) and inverse kinematics. In the case of inverse kinematics, manipulating one of the five control bones (hands, feet, and torso) led to corresponding movement in the child bones (e.g., moving the hand would cause the entire arm to move).
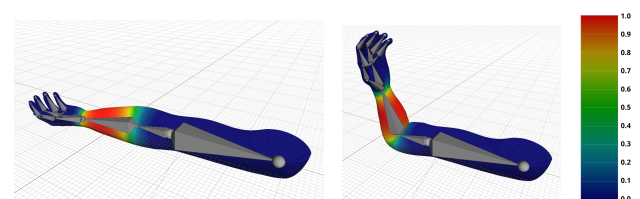

Figure 3: Example of motion and weight painting system for isolated arm with colorbar.

The model was integrated with an STL of a Canyon racing bike. Leveraging the rig, the final position of the cyclist was achieved, preparing it

for printing.

3D Printing

Due to size limitations in the wind tunnel testing, the cyclist was printed at a quarter scale. The printing process took place in the Prototyping Laboratory at Politecnico di Milano (Lecco campus) using the Formiga P-110 3D Printer. Nylon 12 (or PA12), a polyamide material with a density of 1.01 g/cm^3, was employed for printing. With a volume of 1.326×10^3 cm^3, the total weight of the model was 1.397 kg. Using Autodesk Netfabb software, the model was divided into three parts to fit the printer's dimensions, and a perforated cube was added at the bottom bracket position to ensure interconnection with the wind tunnel test section support.
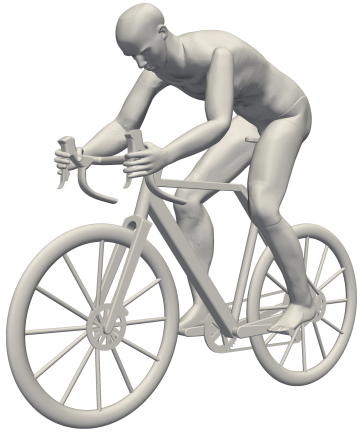

Figure 4: Final position of cyclist in Blender.

3. Wind tunnel

Wind tunnel measurements were necessary to compare the CFD results of the cyclist and to give stability to the further positions analysis. The test results are not reported in this paper as the tests were scheduled to be conducted after the thesis submission deadline. However, the results will be presented in the near future. The experiment took place in the Aerodynamic Laboratory of Politecnico di Milano, in which there is a closed circuit wind tunnel. The cross-section of the test section is W×H=1.5×1 m^2. Being manufactured at 1/4 scale, no corrections were needed for the blockage ratio of the cyclist, in this case equal to 7%.

Figure 5: 3D printed model of the cyclist and model integrated with the wind tunnel setup and transducers.

4. CFD

4.1. Model

Computational domain and geometry

All simulations were performed using Open-Foam. The mesh domain, resulting in a volume of $30.52 \times 15 \times 8.64$ m^3, was generated using BlockMesh and the SnappyHexMesh utility. Seven refinement boxes were created to improve accuracy in capturing the volumes near the cyclist and the wake. The topology of the mesh is depicted in Fig. 6. The 3D RANS equations were solved using the SimpleFoam solver, which is steady-state and incompressible, with the k-ω SST turbulence model. Simulations were conducted for 3000 pseudo-steps of 1 s to ensure convergence, and the results were computed by averaging the last 1000 iterations.
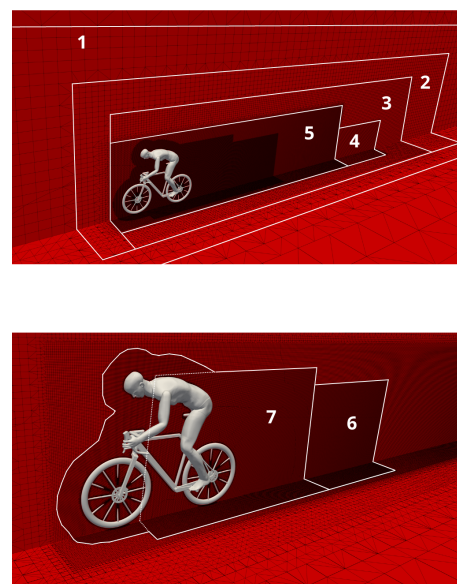

Figure 6: Computational grid with highlight of the seven refinement boxes.

At the inlet, a fixed value was set for the uniform velocity: 15 m/s for the grid independence study and position analysis, and 10 m/s for wind tunnel validation. The wheels were fixed with a rotating wall velocity determined by the equation $\omega = \frac{V}{R}$, where R is the wheel radius of 0.342 m. The center of rotation was aligned with the wheel's axis. For the cyclist and bike frame, a fixed value of 0 m/s was imposed, similar to the bottom of the domain. At the outlet, a zero static gauge-pressure condition was applied.
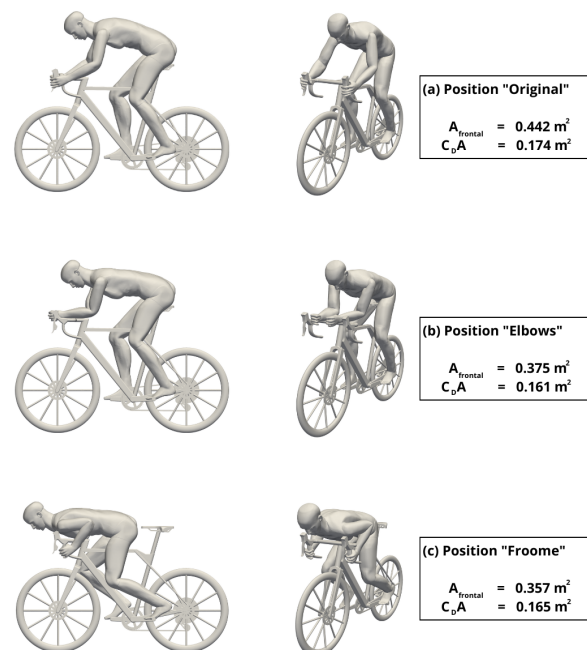
4.2. Grid independence study

The grid was chosen based on a grid sensitivity analysis. Three different meshes were set to perform the independence study. The first one generated was the "Fine", with 70'550'710 cells. Therefore, gradually decreasing the refinement level in the different boxes, the coarser grid were generated. The "Medium" resulted in 22'314'834 cells, while the "Coarse" in 7'017'083 cells. The study was based on the Grid Convergence Index (GCI) to check whether the results were in the asymptotic range of convergence. The parameter of interest was the drag area $(C_D A)$, computed for the three meshes with a refinement ratio approximately equals to 3. Result was in the asymptotic range of convergence, and given that the relative error between the medium and the fine resulted in 0.57%, the medium grid was selected, due to its lower computational cost.

4.3. Position analysis

Once the grid was established, the CFD simulations were set up. The use of Blender to rig the model provided a wide range of analysis possibilities. In particular, the focus was on investigating the aerodynamic of six different cyclist positions with static legs (where the pedaling effect is not taken into account since the difference for a cyclist with crank horizontal is minimal [4]), inspired by Blocken's research on fifteen different cyclist hill descent positions to determine the optimal configuration [2]. However, this research takes a different approach by using a workflow that significantly reduces the time required for this step. The advantages of this approach are numerous: the virtual model created through scanning and rigging is a faithful replica of the real athlete, allowing for natural

movement with the help of the skeleton created through rigging. Recreating the configurations takes less than ten minutes each, and an athlete who wants to analyze the aerodynamics of a position change does not need to be physically present for additional scans or wind tunnel tests. Instead, they can obtain results from their virtual model. Therefore, the primary goal of this section is not to determine the optimal aerodynamic descent position for a cyclist, but to showcase the convenience and ease of working with a virtual model created through scanning and rigging. Five additional configurations, obtained by manipulating the cyclist in Blender, are compared in this section. The same motion system used to create the initial position was employed, controlling the five end-effectors (inverse kinematics) and rotating bones (forward kinematics), such as those of the fingers.

The positions are shown in Fig. 7: (a) represents the "Original" position, used for 3D printing, and employed in the grid independence study; (b) is the "Elbows" position, where the hands no longer hold the handlebar, but instead rest on it; (c) "Froome" and (f) "Pantani" depict the iconic positions of the two famous athletes with the same names; (d) is the "Aero" position, similar to the "Original" but with a more inclined back aligned with the flow direction; finally, (e) represents the "Superman" position, which is not allowed in current UCI racing competitions but was included due to its distinctive nature.

(a) Position "Original"

$A_{frontal}$ = 0.442 m²
$C_D A$ = 0.174 m²

(b) Position "Elbows"

$A_{frontal}$ = 0.375 m²
$C_D A$ = 0.161 m²

(c) Position "Froome"

$A_{frontal}$ = 0.357 m²
$C_D A$ = 0.165 m²

(d) Position "Aero"

$A_{frontal}$ = 0.368 m^2
C_DA = 0.168 m^2

(e) Position "Superman"

$A_{frontal}$ = 0.285 m^2
C_DA = 0.129 m^2

(f) Position "Pantani"

$A_{frontal}$ = 0.351 m^2
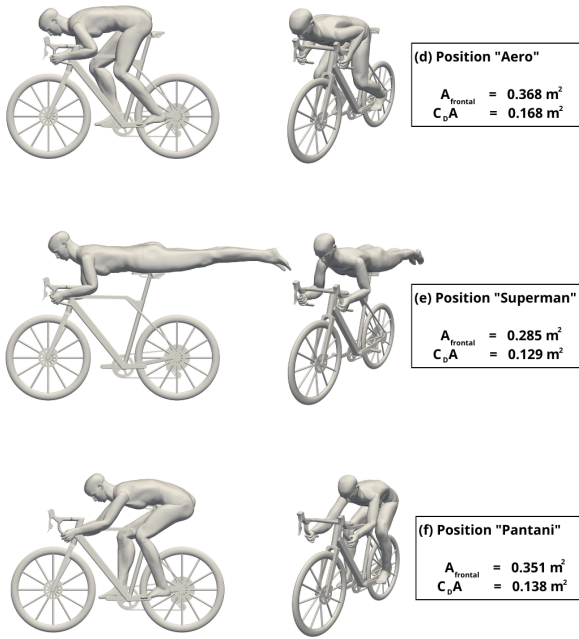C_DA = 0.138 m^2

Figure 7: Side views and perspective views of the six positions. Frontal area and drag area are indicated.

Fig. 8 illustrates the six positions in terms of drag area and frontal area. The aerodynamic superiority is evident in the "Superman" position, as expected, due to its significantly smaller frontal area. The second-best position is "Pantani", which is not as aerodynamically efficient as the "Superman" but still outperforms the other four configurations.
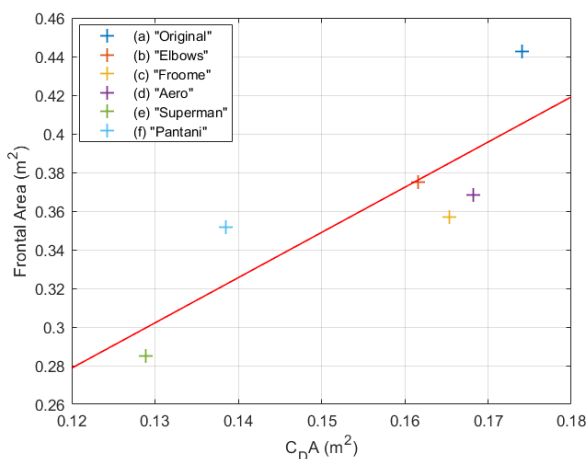

Figure 8: Drag area versus frontal area for all 6 positions, and mean trend line

The "Original" position, as anticipated, performs the worst since it was not aerodynamically optimized. Comparing "Elbows", "Froome,"

and "Aero" all three exhibit significantly higher drag areas compared to "Pantani." However, having a higher (lower) frontal area does not necessarily translate to a higher (lower) drag area. Among these three positions, "Elbows" has the smallest drag area, despite having the highest frontal area. The graph also displays the line of best fit, the straight line that minimizes the distance between the line and data points. This line helps visualize the performance of different configurations compared to the mean trend. Configurations above the line, such as "Pantani" and "Original" positions, perform better, while those below the line, like "Froome," "Aero", and "Superman", perform worse than the mean trend. This suggests that the optimal aerodynamic position for a given frontal area may differ from the mean trend. Further insights into the reasons for the differing aerodynamic behaviors can be gained from analyzing the distribution of the total pressure coefficient ($C_{p_{tot}}$) across the surfaces of the cyclist and bike. The $C_{p_{tot}}$ distribution and isosurfaces for a total pressure coefficient of zero are presented for each configuration. The distribution is plotted within a range rescaled from -1 to 1, divided into twelve colored subranges to enhance visibility. The isosurfaces visually depict the regions where the drag is generated, as they enclose a low-pressure bubble that creates resistance and slows down the cyclist.

(a) "Original" position

(b) "Elbows" position

The "Original" position is characterized by having the largest area of high $C_{p_{tot}}$ among the six configurations. These areas are located at the

front of the cyclist, while the largest separation bubbles are generated at the back, which explains the poor aerodynamic performance.
(c) "Froome" position

(d) "Aero" position

(e) "Superman" position

(f) "Pantani" position

Figure 9: Total pressure coefficient on cyclist and bicycle surfaces, and isosurfaces for $C_{p_{tot}} = 0$

In the "Elbows" configuration, the position of the arms acts as a shield for the upper body, resulting in a minor contribution to the resistance force. Although the flow is still perturbed by the presence of the arms, less of the torso and legs face the oncoming wind due to this shielding effect.
The "Superman" position exhibits the least area of low values of $C_{p_{tot}}$. These zones are only present along the side of the left arm but do not contribute to drag since the generated force is directed perpendicular to the flow velocity. There are only a few areas of separation, as the horizontal alignment of the body in this position

prevents the lower back from generating any significant separation bubble. The flow remains attached to the body surface until the foot.
The "Pantani" position is characterized by the longest bubble generated at the back, indicating a strong pull-back effect in this region. However, there are not many other body surfaces that lead to separation, particularly the position of the legs, which seems to avoid creating low-pressure zones. The effectiveness of this configuration is likely due to the particular position of the arms. The angle between the lower and upper arms is not too high, resulting in a more streamlined configuration and fewer separation bubbles.

5.   Conclusions

The main focus of this study was to develop a method that allows for conducting cycling aerodynamic tests while reducing the time typically spent by athletes and teams using the traditional method of wind tunnel testing. The workflow was evaluated using a full-size static mannequin for simplicity. The process involved 3D scanning the mannequin and importing the virtual model into Blender software. Through rigging animation techniques, a motion system was created to convert the mannequin's position into that of a cyclist. The model, integrated with a bike, was then quarter-scaled and 3D printed for testing in the wind tunnel to validate the results obtained from CFD simulations of the same model. 3D RANS equation with k-ωSST model was used for solver. To demonstrate the ease of use of this method and its potential application for real athletes, an analysis of six different cyclist positions was conducted, comparing them in terms of drag area and the distribution of the total pressure coefficient. The overall time required for the entire procedure can be summarized as follows:

- Model preparation and scanning: 15 minutes
- Data post-processing in the scanning software: 2 hours
- Rigging and cyclist animation: 1 hour
- Changing positions: 10 minutes

Additionally, the time required for computing CFD simulations should be considered, although it depends on the computational power available. The significant advantage of this approach is that the athlete's involvement is minimal, as

their presence is only required during the scanning step. Subsequent analyses, whether related to changes in position or equipment, can be performed at any preferred time without the limitations of physically coming to the wind tunnel to conduct tests. Regarding the position analysis, despite the variations in cyclist size and structure, bike type, solver, boundary conditions, and the process of recreating the positions, a similar trend to Blocken's findings is observed. Among the six positions, the "Superman" position is found to be the fastest, while the "Original" position is the slowest. The "Pantani" position is the second fastest. The remaining three positions yield drag area values that are very close to each other. Interestingly, the "Froome" position, which has the highest frontal area among the three, is associated with the lowest drag area. This indicates that there is not a direct correspondence between an increase in frontal area and an increase in drag area.

6. Acknowledgements

References

[1] Mark Adams, Erick Miller, and Max Sims. *Inside Maya 5*. 2003.

[2] Bert Blocken, Thijs van Druenen, Yasin Toparlar, and Thomas Andrianne. Aerodynamic analysis of different cyclist hill descent positions. *Journal of Wind Engineering and Industrial Aerodynamics*, 181:27–45, 2018.

[3] RB Candau, F Grappe, M Ménard, B Barbier, GY Millet, MD Hoffman, AR Belli, and JD Rouillon. Simplified deceleration method for assessment of resistive forces in cycling. *Medicine and science in sports and exercise*, 31(10):1441—1447, October 1999.

[4] Timothy N. Crouch, David Burton, Mark C. Thompson, Nicholas A.T. Brown, and John Sheridan. Dynamic leg-motion and its effect on the aerodynamic performance of cyclists. *Journal of Fluids and Structures*, 65:121–137, 2016.

[5] TU Delft. A 3d printed mannequin of tom dumoulin in the tu delft wind tunnel helps gain a competitive advantage, 2016.